Appendix F
Measurement of the Absolute Populations of Excited Atoms by Classical Spectroscopy Techniques

Written by Prof. Yu. B. Golubovskii

In plasma spectroscopy, the populations of excited atoms are frequently measured by the classical (other than laser) light emission and absorption methods. At the foreground in that case is the problem of adequate illumination of the spectral instrument and the correct calculation of the luminous flux that in the final analysis reaches the detector. The specificity here is that plasma sources are, as a rule, extensive and volumetric. The luminous flux from volumetric plasma sources is compared with that from standard sources, frequently in the form of flat tungsten-ribbon photometric lamps. The radiation of such a standard source can be characterized by the surface brightness b_λ [$\mathrm{Wcm^{-2} \cdot Å \cdot sr}$] – the power emitted by a unit surface area into a unit solid angle within a unit wavelength interval in a direction normal to the area – or by the radiance r_λ [$\mathrm{Wcm^{-2} \cdot Å \cdot sr}$] – the emission of a unit surface area into a solid angle of 2π. The relation between brightness and radiance for cosine radiators is well known to be $r_\lambda = \pi b_\lambda$. By comparing between the luminous fluxes from plasma and the standard source, which have been made to travel one and the same optical path by means of a tilting mirror, one can deduce the absolute spectral line intensity $I_{i,k}$ [$\mathrm{Wcm^{-3}}$] or the continuum intensity I_λ [$\mathrm{Wcm^{-3} \cdot Å}$], that is, the power emitted by a unit volume of plasma into a solid angle of 4π, either integrally, in the spectral line, or within a unit wavelength interval in the continuum. The population N_i [$\mathrm{cm^{-3}}$] of the emitting level is then found from the absolute spectral line intensity by the relation $I_{i,k} = N_i A_{i,k} h\nu_{i,k}$, where $A_{i,k}$[$\mathrm{s^{-1}}$] is the transition probability and $h\nu_{i,k}$ is the quantum energy. The traditional scheme of the experiment is shown in Figure F.1.

When taking measurements with a high spatial resolution, one should use a good objective lens, corrected for various kinds of aberrations, to project a reduced real image of the volumetric plasma source onto the entrance slit of the spectral instrument. In the plane of the slit is formed a sufficiently sharp real image of the source, because the image reduction in the longitudinal direction is squared that in the transverse direction.

Spectroscopy of Low Temperature Plasma. Vladimir N. Ochkin

ISBN: 978-3-527-40778-1

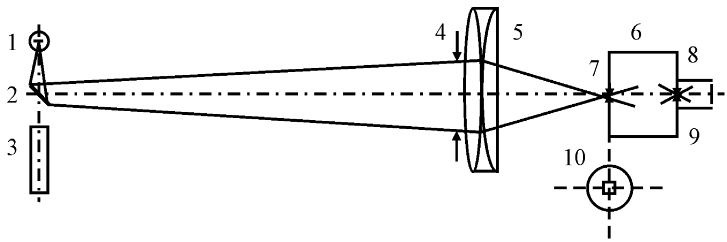

Figure F.1 Schematic of absolute line intensity measurements: 1 – standard source (a photometric lamp); 2 – tilting mirror; 3 – plasma source (e.g. a discharge tube); 4 – objective lens diaphragm; 5 – objective lens; 6 – spectral instrument; 7 and 8 – entrance and exit slit, respectively; 9 – radiation detector; 10 – image (scaled up) of the plasma object in the slit plane.

Indeed, if one uses the thin lens formula and differentiates,

$$\frac{1}{x} + \frac{1}{x'} = \frac{1}{f}; \quad \frac{\Delta x}{\Delta x'} = -\frac{x^2}{x'^2},$$

one can then see that if the image reduction is defined by the ratio $-x'/x$, the ratio between the longitudinal dimensions of the image and the object is reduced squared number of times more (x, x' are conjugate points, f is the focal length of the objective lens). The minus signs mean that the image will be reversed and inverted (the near and far sections will change places). We can cite a typical example of measurements of the radiation intensity using the positive column of a discharge 20 mm in diameter and 40 cm long. Let the image of the discharge tube reduced by a factor of 7 be projected onto the slit of the spectral instrument by means of an objective lens 25 mm in focal length. The reality of measurements is that the flat tungsten ribbon of the standard source is projected onto the plane of the slit absolutely sharp (up to the aberrations of the lens), whereas different sections of the volumetric source prove to be out of focus in the plane of the slit, except for the section whose distance from the objective lens coincides with that of the tungsten ribbon. This section is assumed to be coincident with the center of the discharge tube and 200 cm distant from the objective lens, with the given focal length and 7-fold image reduction. Accordingly, the front and rear windows of the discharge tube will be 180 cm and 220 cm distant from the objective lens. In the image plane, they will be 28.2 cm and 29 cm distant from the lens, while the plane of the slit, 28.6 cm remote from it. The front window will be reduced by a factor of 6.38, whereas the rear one, 7.58 times. The image of the discharge tube will look like a conical layer of small thickness, a mere 8 mm, and will be perceived as a sharp image of an object in the form of a circle some 3 mm in diameter. It is expedient to place two crossed slits at the entrance, which will make it possible to isolate from the image the region of interest with a high (no worse than 0.01 mm) accuracy. It will then be possible to isolate from this circle a small area, say 2 mm by 2 mm in size, and set the diaphragm of the objective to approximately 2 cm diameter, so as to match the angular dimensions to the relative aperture of the spectral instrument (1:10 in our example). In that case, the solid angle through which the light from the sources is collected turns out to be small enough. This scheme of illumination of the spectral instrument provides for a sufficiently good spatial resolution, which will be discussed later in the text.

The prime task facing the experimenter is to correctly calculate the differential luminous fluxes issuing from various elementary plasma volumes and integrate them over that plasma region, whose light passes through the slit of the spectral instrument. The next, simpler step is to calculate the luminous flux from the photometric lamp that has passed through the slit. Taking the ratio between these fluxes, which are proportional to the signals registered from plasma and from the standard source, one can determine the absolute intensity of the spectral line or continuum.

This problem can be solved by two equivalent methods. First of all, it is necessary to find the locus of points of the volumetric source, from which light enters the spectral instrument. Next, as already mentioned, it is necessary to calculate the luminous flux from an elementary plasma volume, with due regard for absorption in the source, and finally, integrate over the locus found, allowing for the possible spatial inhomogeneity.

The second method consists in calculating the illuminance in the plane of the slit produced by some section of the volumetric source (in the general case, the image will be out of focus), summing up the illuminances from all the sections of the source, and finally, integrating the total illuminance over the area of the slit. Naturally both these methods yield the same final results.

Let the reduced image of the volumetric source be projected into the slit plane P' as shown in Figure F.2. The coordinates are reckoned from the principal planes of the optical system. The plane P, conjugate to P', is projected exactly into the slit plane with a reduction of a'/a. Let us isolate an elementary volume $\mathrm{d}V$ with the coordinates x, r within the limits of the source in the plane P_1, which is projected into the point x', r' in the plane P_1', and find the luminous flux that passes from the elementary volume $\mathrm{d}V$ through the elementary area $\mathrm{d}\sigma'$ of the slit on the optical axis of the system. The luminous flux is captured by the objective lens within the solid angle Ω and, propagating in the image space, forms a uniformly illuminated circle of radius ρ in the slit plane, the center of

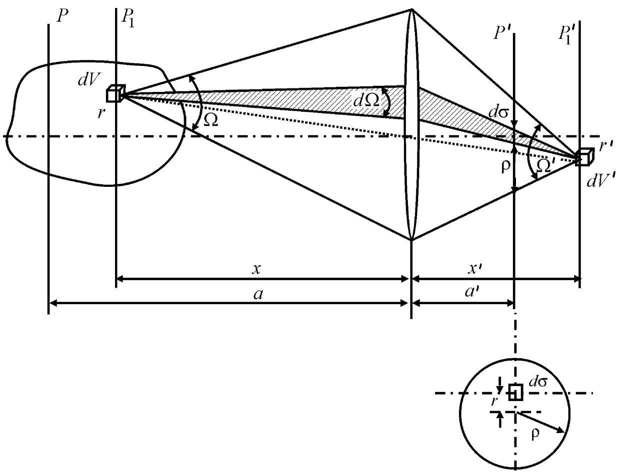

Figure F.2 To the calculation of the luminous flux entering the spectral instrument through the elementary area on the optical axis in the slit plane.

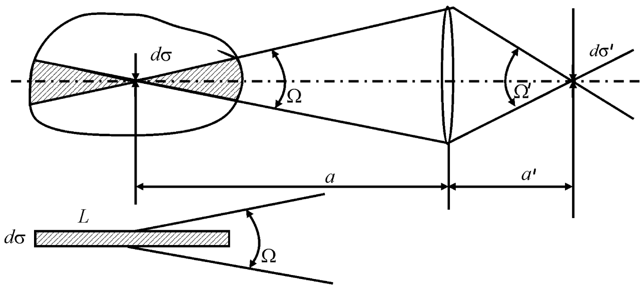

Figure F.3 Conical surface cutting out that volume in the plasma source, from which light enters the spectral instrument through the center of the slit (top). Cylindrical volume equivalent to the cone in calculating the luminous flux (bottom).

this circle lying at a distance of r'' from the optical axis (bottom part of Figure F.1). Obviously, light will pass through the elementary area $d\sigma'$ only if the condition $r'' \leq \rho$ is satisfied. This condition determines the locus of those points of the source, light from which enters the spectral instrument through the small area $d\sigma'$. In actual experiments, the solid angles Ω, Ω' are small enough, so that the paraxial optics approximation can be used. Using the similitude of triangles and expressing the primed coordinates in terms of the unprimed ones by the rules of geometrical optics, one can write down, accurate up to second-order, terms of the condition for the passage of light through the slit of the spectral instrument in the form

$$r \leq R\left(1-\frac{x}{a}\right).$$

This expression describes in the space of the object a conical surface with vertex at the point $x = a$, which rests on a circle of radius R on the surface of the objective lens as on a base (Figure F.3). Since it is only a fraction of the luminous flux, equal to the ratio $\mathrm{d}\sigma'/\pi\rho^2$, that will pass through the elementary area $\mathrm{d}\sigma'$ of the slit (which is equivalent to the capture of the luminous flux within a small solid angle $\mathrm{d}\Omega$ shaded in Figure F.1), the luminous flux gathered from the elementary volume $\mathrm{d}V$ turns out to be

$$\mathrm{d}F = \frac{I\mathrm{d}V}{4\pi}\Omega(x)\frac{\mathrm{d}\sigma'}{\pi\rho^2(x)}. \tag{F.1}$$

The total flux that has passed through $\mathrm{d}\sigma'$ is obtained by integrating over the conical surface. For a homogeneous and nonabsorbing source, we have

$$F = \frac{I}{4\pi}\frac{\mathrm{d}\sigma'}{\pi}\int_0^{2\pi}\mathrm{d}\varphi\int_{a-L/2}^{a+L/2}\left(\frac{\Omega(x)}{\rho^2(x)}\int_0^{R(a-x)/a} r\,\mathrm{d}r\right)\mathrm{d}x. \tag{F.2}$$

Integration with respect to φ gives 2π. Considering that

$$\Omega(x) = \pi R^2/x^2; \quad \rho = R\frac{f(a-x)}{x(a-f)},$$

we get an interesting corollary, namely, the integrand in x

$$2\pi\frac{\Omega(x)}{\pi\rho^2(x)}\frac{1}{2}r^2\bigg|_{0}^{R(a-x)/a} = \pi R^2\left(\frac{a-f}{af}\right)^2 = \frac{\pi R^2}{a'^2} = \Omega' \tag{F.3}$$

is independent of the coordinate x and is equal to the solid angle Ω' at which the objective is viewed from the point $\mathrm{d}\sigma'$. Integration with respect to x is in this case reduced to multiplication into the length L of the source, and finally it follows from formula (F.2) that

$$F = I\mathrm{d}\sigma' L\frac{\Omega'}{4\pi} = I\mathrm{d}\sigma L\frac{\Omega}{4\pi}, \tag{F.4}$$

where $\mathrm{d}\sigma = \mathrm{d}\sigma'\left(a/a'\right)^2$ is the element of the area $\mathrm{d}\sigma'$ scaled into the image space with a magnification of $\left(a/a'\right)^2$ and $L\mathrm{d}\sigma$ is the volume of a cylinder of length L and base area $\mathrm{d}\sigma$. This result shows that, subject to the assumptions made above, the luminous flux gathered from any section of the cone within the limits of the volumetric source is the same. Only small fractions of light, equal to $\mathrm{d}\sigma'/\pi\rho^2$, pass from elementary

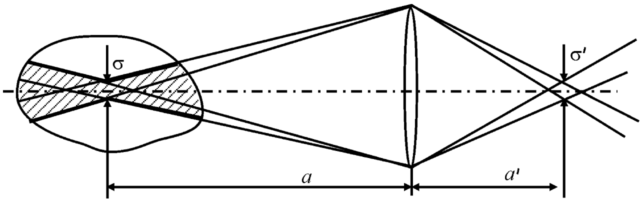

Figure F.4 Conical surface cutting out that region of the source, from which light enters the spectral instrument through a finite-size slit.

volumes in the unfocused image, but these volumes are sufficiently numerous for these two factors to be completely offset for any section of the volumetric source. Thus, for the illumination scheme under consideration, a cone inscribed in the volumetric source is totally equivalent to a cylinder of length L and base area $d\sigma$, the luminous flux from each element of the cylinder being gathered through a solid angle of $\Omega = \pi R^2/a^2$ (shaded region in the bottom part of Figure F.3). The effective diaphragm radius R can be determined either by the diameter of the objective lens or by the relative aperture of the spectral instrument, for the angle Ω' can be limited by the collimator of a spectrograph.

Figure F.2 shows the region of the volumetric source, whose light passes through the elementary area $d\sigma'$ of the slit, which is located on the optical axis (the vertex of the cone coincides with $d\sigma'$, point slit approximation). If the slit is of finite size σ', light passing through the other elementary areas of the slit will be gathered from the cones whose vertices coincide with the images of these areas in the space of the object. To calculate the luminous flux that has passed through the slit of finite size, it is necessary to swing the optical axis from one edge of the slit to the other. The region from which radiation enters the spectral instrument in the case of finite-size slit is shaded in Figure F.4. This region determines spatial resolution in absolute measurements. One can demonstrate that in this case, analogy also holds between the cone from Figure F.3 and a cylinder with a length of L and a cross-sectional area of σ equal to the total area σ' of the slit increased by a factor of $(a/a')^2$. In actual experimental conditions, spatial resolution is of the order of a millimeter and can be bettered to a few fractions of a millimeter, depending on the size of the slit and the effective diaphragm. As in any physical experiments, the improvement of spatial resolution worsens the signal-to-noise ratio at the output of the recording system, and so a reasonable trade-off decision is required in selecting the parameters of the optical system.

With the luminous flux calculation scheme suggested, one can easily introduce corrections for the axial inhomogeneity within the limits of the source if one puts $I(x) = I_0\Psi(x/L)$, where I_0 is the maximum intensity and the function Ψ describes the relative axial radiation intensity distribution. Obviously the magnitude of the luminous flux is in this case given by

$$F = I_0 \mathrm{d}\sigma L \frac{\Omega}{4\pi}\psi; \quad \psi = \frac{1}{L}\int_{a-L/2}^{a+L/2} \Psi\left(x/L\right)\,\mathrm{d}x. \tag{F.5}$$

The radial inhomogeneity in the given illumination scheme can be disregarded at small angular apertures.

As applied to an axially symmetric source viewed across the axis (Figure F.5), expression (F.5) assumes the form

$$F(y) = I_0 \mathrm{d}\sigma R_0 \frac{\Omega}{4\pi}\psi(y); \tag{F.6}$$

$$\psi(y) = 2\int_0^{\sqrt{1-y^2}} \Psi(r)\mathrm{d}x = 2\int_y^1 \frac{\Psi(r)\mathrm{d}r}{\sqrt{r^2-y^2}}. \tag{F.6a}$$

The relative coordinates x, y, r range between 0 and 1, I_0 is the absolute radiation intensity at the center of the source, $\psi(y)$ is the measured relative transverse distribution normalized to unity at the center and $\Psi(r)$ is the relative radial intensity distribution. To convert from the measured transverse distribution $\psi(y)$ to the true radial distribution $\Psi(r)$, it is necessary to solve Abel's equation (F.6)a by any of the numerous methods developed for the purpose.

Spatial resolution can be improved with the aid of the instrument function that describes the broadening of a delta-shaped point source in the course of projection into the plane of the slit. Indeed, the aberrations of the projection optics and the finite sizes of the slits and effective diaphragms result in instrumental distortions as regards spatial measurements. The instrument function is rather difficult to calculate, but its form can be easily found by replacing the volumetric with by a point one and scanning its image in the actual experimental setup. The instrument function thus obtained should be normalized to unit surface area. In that case, the measured radial distribution $F'(r)$ will be related to the true distribution $F(r)$ by the convolution-type equation

$$F'(r) = \int F(\rho)A(r-\rho)\,\mathrm{d}\rho.$$

To exclude instrumental distortions, use can be made of the well-developed methods for solving ill-posed problems. Allowing for instrumental distortions is especially important when measuring luminous fluxes across the axis in axially symmetric sources (Figure F.5). One

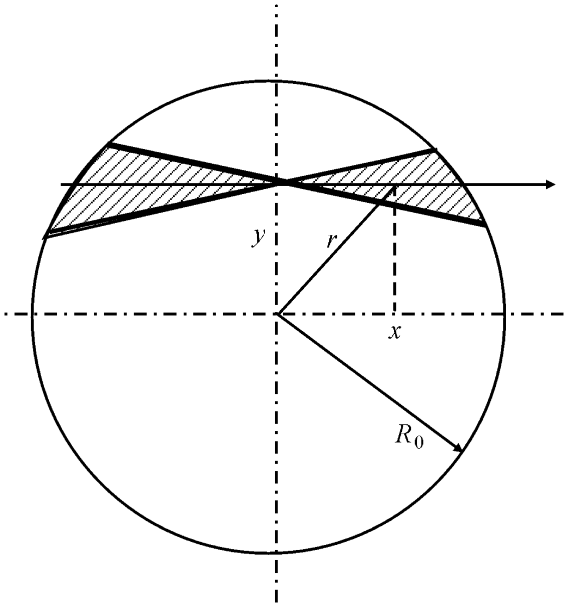

Figure F.5 Luminous flux gathered from an axially symmetric source viewed across the axis.

should first correct the observed transverse distribution for the spatial instrumental distortions and then take the Abelian transformation to get the true radial distribution. One has to deal here with the successive solution of two first-order integral equations, which is generally a complex enough problem. Figure F.6 presents some illustrative examples showing what instrumental distortions one can expect when measuring radial line intensity distributions along and across the axis of a discharge. For example, when studying the radial structure of a contracted discharge filament 3 mm in radius, the radial distribution measured along the axis is $F'(r)$ (Figure F.6a). The instrument function is approximated by a Gaussian curve with a half-width of 1 mm. Following correction for the instrumental distortions, one gets the curve $F(r)$ which at maximum differs by ca. 30% from the measured one. The transverse distribution measured across the axis (Figure F.6b) is $\psi(y)$, and the radial distribution recovered from it without correction made for the instrumental distortions is $\Psi_1(r)$, while that recovered with due regard for the distortions, $\Psi_2(r)$. Taking account of instrumental distortions is especially important where plasma glow is concentrated in peripheral regions, for example, in the case of skin effect. In that case, the effect of instrumental distortions in the analysis of the spatial structure of a plasma source can be appreciable.

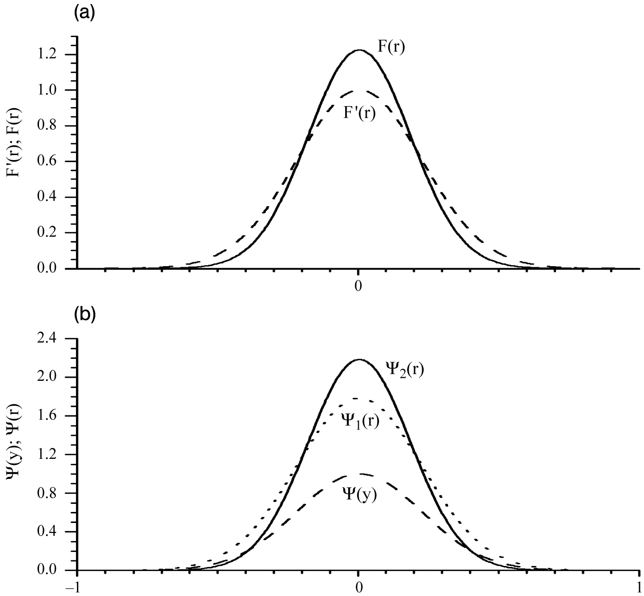

Figure F.6 Illustrating the effect of instrumental distortions when taking spatial luminous flux measurements for an axially symmetric source viewed (a) along and (b) across the axis. $F'(r)$ and $F(r)$ – observed and recovered radial distributions for the source viewed along the axis, $\psi(r)$ – observed transverse distribution, $\Psi_1(r)$ – radial distribution recovered without allowing for instrumental distortions, $\Psi_2(r)$ – radial distribution recovered with due regard for instrumental distortions.

This luminous flux calculation method makes it possible to easily take account of self-absorption within the limits of an axially homogeneous source. To this end, one should multiply expression (F.1) into the probability that quanta will cover the distance from the point with the coordinates x, r to the boundary of the source without being absorbed and then integrate it over the conical surface. The probability that the quanta emitted in a spectral line with an emission profile of ε_ν will cover the distance x without being absorbed is

$$w(x) = \int_0^\infty \varepsilon_\nu \exp(-k_\nu x)\mathrm{d}\nu, \tag{F.7}$$

where $k_\nu$is the absorption line profile, $\int_0^\infty \varepsilon_\nu \mathrm{d}\nu = 1$.

It proves convenient to move the origin of coordinates to the point $x = a$. Multiplying expression (F.1) by (F.7) and integrating over the conical surface with due regard for property (F.3), we get

$$F = I\mathrm{d}\sigma\frac{\Omega}{4\pi}\int_{-L/2}^{L/2}\mathrm{d}x\int_0^\infty \varepsilon_\nu \exp\left(-k_\nu\left(\frac{L}{2} - x\right)\right)\mathrm{d}\nu. \tag{F.8}$$

Changing the order of integration and integrating with respect to the coordinate, we have

$$F = I\mathrm{d}\sigma L\frac{\Omega}{4\pi}\int_0^\infty \frac{\varepsilon_\nu}{k_\nu L}\left(1-\exp\left(-k_\nu L\right)\right)\mathrm{d}\nu \equiv I\mathrm{d}\sigma L\frac{\Omega}{4\pi}S(k_0L), \tag{F.9}$$

where $S(k_0L)$ is the Ladenburg function and k_0 is the absorption coefficient at the line center. Expression (F.9) gives in absolute measure the magnitude of the luminous flux that has passed through the slit of the spectral instrument from the volumetric plasma source in the given illumination scheme in the presence of reabsorption within the limits of the source.

The Ladenburg function shows how much the luminous flux emitted by the plasma column of fixed length is reduced as the absorption coefficient grows higher. The product of the column length and the Ladenburg function shows how the radiant flux increases with increasing column length at a fixed absorption coefficient. The integrand in expression (F.9) shows how the spectral line profile deforms outside of the source as the optical density is increased. Obviously expression (F.9) becomes (F.4) if one puts $k_\nu \to 0$ and expands the exponent in the integrand in (F.9) into a series. Passage to the limit of high absorption coefficient values is not so obvious. If one simply neglects the exponent in comparison with unity in expression (F.9), then, assuming similar emission and absorption line profiles, one obtains divergence on integrating with respect to frequency between infinite limits. The important point is that despite the great optical thickness near the line center, absorption in the far wings of the line becomes weak, the exponent approaches unity and cannot be omitted when taking the integral in expression (F.9). Actually this means that photons in the line wings can move large distances without being absorbed and leave the plasma volume. One can expunge the divergence if one formally cuts off the spectral line wings at some fixed frequencies. In this hypothetical case, integration over a finite spectral interval, with the exponent disregarded and the emission line profile normalization taken into account, yields

$$F = I\mathrm{d}\sigma\frac{\Omega}{4\pi}\frac{1}{k_0},$$

and the luminous flux no longer depends on the length of the source. For real line profiles, the Ladenburg functions fail to reach saturation. Figure F.7 presents the luminous flux issuing from a plasma column as a function of the column length at a fixed absorption coefficient.

To confine the emission of spectral lines within the volume of plasma, it is necessary to introduce stimulated transitions along with the spontaneous ones and to take into account the broadening and overlapping

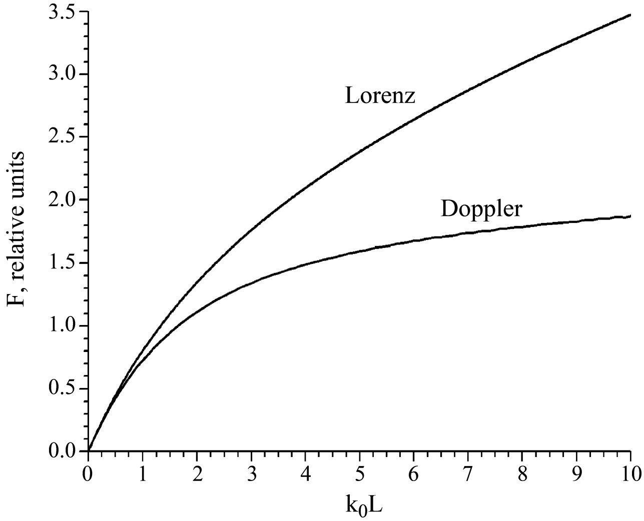

Figure F.7 Luminous flux as a function of the discharge column length at a fixed absorption coefficient for a Doppler and a Lorentz line profile.

of spectral lines. In this case the intensity in the line center will be equal to the Planck's blackbody intensity value. Based on expression (F.9), one can construct classical methods for measuring the densities of emitting atoms, which was started by Ladenburg and co-workers and described in many books on plasma spectroscopy.

Formula (F.4) for an optically thin source and (F.9) for a source with self-absorption can be used to calculate the absolute intensities of spectral lines. To this end, it is necessary to calculate the luminous flux that has passed through the slit from a standard source to be located at a distance of a from the objective lens, which is attained by means of a tilting mirror. Let S be the surface area of the ribbon filament of the photometric lamp and $b = \int_0^\infty b_\lambda \, d\lambda$, the integral brightness determined from the ribbon temperature specified in the lamp certificate, depending on the filament current. The luminous flux that has been gathered by the objective lens and passed through the slit with a surface area of $d\sigma'$ is obviously

$$F_{\rm st} = bS\Omega \frac{d\sigma'}{S'} = b d\sigma' \left(\frac{a}{a'}\right)^2 \Omega = b d\sigma \Omega.$$

This expression is tantamount to the statement that the image brightness is equal to the brightness of the object. The luminous flux issuing from the spectral instrument's exit slit with a width of δl will be

$$F_{\mathrm{st}} = b_\lambda \left(\frac{\mathrm{d}\lambda}{\mathrm{d}l}\right) \delta l \mathrm{d}\sigma\Omega \sim u_{\mathrm{st}} \tag{F.10}$$

where $\left(\frac{\mathrm{d}\lambda}{\mathrm{d}l}\right)$ is the dispersion of the spectral instrument and u_{st} is the registering system signal proportional to the luminous flux from the standard source. If the width of the spectral line emitted by plasma is much smaller than the spectral width of the exit slit, the signal u_{pl} from the plasma source will be proportional to the luminous flux F that in its turn is determined by the integral line intensity I (formulas (F.4) and (F.9)). If we take the ratio between the luminous fluxes registered from the plasma and the standard source, we will have, on canceling out the geometrical factors identical in both cases, the following simple expressions for calculating the absolute intensities of spectral lines:

- for optically thin sources,

$$I = 4\pi b_\lambda \left(\frac{\mathrm{d}\lambda}{\mathrm{d}l}\right) \delta l \frac{1}{L} \frac{u_{\mathrm{pl}}}{u_{\mathrm{st}}}, \tag{F.11}$$

- for sources with reabsorption,

$$I = 4\pi b_\lambda \left(\frac{\mathrm{d}\lambda}{\mathrm{d}l}\right) \delta l \frac{1}{L} S(k_\nu L) \frac{u_{\mathrm{pl}}}{u_{\mathrm{st}}}. \tag{F.12}$$

When registering a continuous spectrum from an optically thin source, the luminous flux passing trough the exit slit of small spectral width will be

$$F = I_\lambda \left(\frac{\mathrm{d}\lambda}{\mathrm{d}l}\right) \delta l \mathrm{d}\sigma L \frac{\Omega}{4\pi}.$$

From the ratio between the luminous fluxes from plasma and the standard source we have the following expression for the absolute intensity of the continuum at a wavelength of λ:

$$I_\lambda = 4\pi b_\lambda \frac{1}{L} \frac{u_{\mathrm{pl}}}{u_{\mathrm{st}}}. \tag{F.13}$$

Thus, formulas (F.11) through (F.13) enable one to calculate the absolute intensities of spectral lines and continua and determine the populations of emitting atoms, and expression (F.9) can help one to get the populations of absorbing atoms when using the classical absorption methods described in Chapters 3 to 5.

References

1 Yu. B. Golubovskii, R.V. Kozakov *et al.* *Phys. Rev.*, **E62**, p. 2707 (2000).

2 S.E. Frish. *Optical Spectra of Atoms* (in Russian). Moscow-Leningrad: Fizmatgiz. (1963)

3 S.E. Frish, Ed. *Gas-Discharge Plasma Spectroscopy* (in Russian). Leningrad: Nauka (1970).

Index

Λ-doubling sublevels 330, 332, 333

a

Abel equation 73
absolute measurements 28, 47
absorption coefficient 12, 24
absorption function 76, 79, 80, 82
absorption spectra of the CO_2 molecules in a discharge 283
acousto-optic spectrometer 435, 437
actinometric pairs 293
actinometry technique 289
adiabatic approximation 176, 230
Airy function 415, 422–424
amplitude of a microwave 329
angular dispersion 409, 410, 413, 416, 417, 432
anharmonicity 192, 194, 195, 198, 202, 208, 209, 214, 217, 221
apodization 428
arcs 456
atomic oscillator 31, 34
atomization 235
autoionization 115

b

black-body radiation 11, 16
Bohr magneton 343
Bohr radius 53
bolometers 465, 474
Boltzmann formula 6
Boltzmann rotational distribution 170
Born–Oppenheimer principle 270
Bose–Einstein statistics 11
Bouguer–Lambert–Beer (BLB) law 44
bound–free transitions 51
bremsstrahlung 52–54, 57–59

c

cavity ringdown spectroscopy 99
characteristic relaxation time 189, 193
charge-coupled devices 481
Clebsch–Gordan coefficient 309
coaxial photocell 467, 474
coherence length 92, 102, 138, 139
coherent anti-Stokes Raman scattering 137, 140

Spectroscopy of Low Temperature Plasma. Vladimir N. Ochkin

ISBN: 978-3-527-40778-1

coherent laser spectroscopy methods 337
collective scattering 377–379, 381, 386
collisional-radiative model 21, 22
complex dielectric constant 398, 399
Compton shift 62
Compton wavelength 309
concentrations of molecular ions 284
concentrations of polyatomic molecules 281
concentrations of the metastable molecules 281
conductivity of the medium 398
continuous spectrum 6, 11, 24, 45, 50
contrast of the image 477
convolution equation 148
coronal approximation 14
coronal ionization equilibrium relation 20
correlations 374, 375
correlations of fluctuation 375
cosine radiator 583

d
Debye screening radius 1
degree of dissociation, ionization, conversion 11
densities of negative ions 298
density matrix formalism 93, 94, 107
density measurements 360, 394
diatomic polar molecules 330
Dicke narrowing 41
diode lasers 88
dipole interaction 312, 313, 332
dipole moment 308, 312, 314, 319, 323, 330–332
discharges along the surface 457
dispersion profile 33
distribution temperature 18
Doppler broadening abnormal 148
Doppler line profile 39, 41, 42, 48, 49
Doppler shift 38, 62
Doppler width 41, 46
dynamic range of electron 360
dynamic Stark effect 345

e
effective inversion temperature 214
effective lifetime approximation 48, 50
Einstein coefficient 44
electric field 307–333, 335–341, 345–349
electric field in an atmospheric-pressure hydrogen discharge 340
electron temperature 18, 20
electron, ion and neutral particle temperatures 17
electronic metastable states 251
electrophotography 479
elliptical orbit 312
emission methods 67
exchange between vibrational quanta 191
excitation of the electron shells of molecules by electrons 174
excitation temperature 19

f

Fabry–Perot interferometer 414, 415, 418, 421–425, 484
Faraday effect 342, 343, 349
Fellgett advantage 429, 430
Fermi interaction 198
fluorescence decay 112, 118
fluorescence induced by synchrotron radiation 120
fluorescence spectrum of the NaK molecule 331
fluorescence-dip detection 336
focal aperture 409, 411, 412, 416
focal plane 409, 410, 412, 414–416, 420, 422, 477, 479
four-photon process 136, 141
four-wave mixing 97, 146
Fourier spectrometer 408, 425, 427, 429, 430, 438
Franck–Condon factor 220
free spectral range 414, 418–421, 427, 428, 437, 438
free–free transition 51
frequency detuning parameter 37
frequency shift 32, 37, 41, 61, 62
frequency-tuned laser 84, 85, 99, 104, 122
Fresnel formula 399, 402
Fresnel number 102
Fulcher series 179

g

gas-discharge lamp 441
Gaunt correction factor 55
Gaussian shape 39
Girard raster 432, 433

h

Hönl–London factor 199
Holtsmark distribution function 358, 359
hot plasma 2, 3
Hund coupling types 509
hydrogen-like atoms 35, 55, 59

i

ideal plasma 3, 9, 11
identification of spectra 67
illumination engineering unit 30
illumination engineering units 439, 440, 462
image converter and intensifier tube 479
incursion 353, 355
inductively coupled plasma 235, 303
Inglis–Teller effect 326
instrument (spread) function 148
integral absorption 200, 202, 212
integral absorption coefficient 44, 45
intensities of the satellites 317
interferometric methods of measuring the density 351
intermodulation optogalvanic spectroscopy 124
internal rotation 494
internal statistical sum 7, 8
intracavity laser spectroscopy 95, 144
intrinsic photoeffect 462, 470, 472, 479, 480
inverse problem 23, 24
inversion of molecular IR band 214
ion broadening parameter 365
ion component of the scattered spectrum 381, 388

ion concentration 268, 288
ion velocities 36
ionization energy 9
ionization potential reduction 9
ionization temperatures 17

j
Jacquinot advantage 421, 438

k
Kirchhoff's law 11, 16
Klein–Nishina formula 61
Kramers formula 54

l
Ladenburg and Levi function 48
Ladenburg and Reiche function 48
Lagrange–Helmholtz principle 30
lambda doubling 271
Landau–Teller relaxation equation 156
Lande factor 343
laser-induced fluorescence 104, 105, 120
law of mass action 7–9
light intensity 28
light scattering 60
light-gathering power 412, 413, 419–421, 428, 430, 431, 436, 438
limit of discernibility of individual lines 368
linear dispersion 410, 417, 421, 437
linear splitting 314
linear Stark effect 34
local electric field 307
local thermal equilibrium 14, 16
Lorentz broadening 32, 36, 41, 46
Lorentz–Lorenz formula 399
Loschmidt number 12

m
magnetic field measurement method 342
magnetic quantum number 323, 328
Maxwell distribution function 6, 21
measurement of the electron density 343
Michelson interferometer 414, 425, 430
Milne formula 57
modified diffusion approximation 226
multipass absorption cells 95, 97, 98
multiphoton fluorescence excitation 334
multiphoton interaction 129
multiplet component 81, 82, 84

n
natural decay 32, 33, 42
noise component 463
noise equivalent power 464
noise factor 86
non-hydrogen-like atoms 364
nonisothermal mixture of particles 167
nonlinear susceptibility tensor 338, 339
nuclear spin 490, 491
nuclear statistical weight 276

o
optical density 29, 44, 46–48, 50

optically thin plasma 20, 24
optico-acoustic detector 466
optogalvanic effect 104, 121–123, 128, 146
oscillator strengths 44, 45

p
parabolic coordinate 312
parity 491
partial equilibria 14
partial local thermal equilibrium 14, 16
partial temperature 17, 21
phase 353–355, 374, 375
phase perturbations 34, 35
phase-matching 138, 139
photocathodes 467, 468
photographic emulsion 472
photoionization 57, 59
photometric parameter 419, 439, 448
photometric quantitie 29
photometric quantity 27
photomultiplier 467–470, 475, 479, 480
photon noise 429, 430, 462
photorecombination 55, 57, 59
photoresistor and photovoltaic detector 470
Planck formula 11, 13
plasma microfield 326
plasma turbulence 316
plasmatron 456
plasmatrons 456
point symmetry group 489, 490
polarizability 351, 352
polarization intermodulation excitation 125
polarization state of the field 322
Poynting vector 12
predissociation 116
probability of radiative transitions in diatomic molecul 269
profile homogeneous 33
profile of the π- and σ-component 344
profile of the D_γ line 317
profile of the H_α spectral line 316
profile of the H_δ spectral line 314
profile of the spectral line 321
pulsed light source 448
pyroelectric detector 465

q
quadratic Stark effect 34–36
quality of a photographic image 477
quantitative spectroscopy 27
quantum efficiency 463, 473
quantum numbers 487
quantum photodetectors 461, 472
quasineutrality 1
quenching cross section 34

r
Rabi frequency 93, 108, 109
radiant emittance 27–29
radiant energy density 27
radiant flux 27, 28, 30
radiation induced by the static 337
radiation transfer 29, 47, 50
Radon integral transformation 72
random processes 32
raster spectrometer 431

ratio between the Thomson and the Rayleigh scattered intensity 383
Rayleigh criterion 411, 418, 478
Rayleigh scattering 63
recombination continuum 51
reduced field 307
reflection and transmission of film 400
reflection coefficient 398, 399, 401, 403–405, 422, 425, 437
refractive index 351, 352
relative intensities of lines in the rotational structure 180
resolving power 409–411, 418, 419, 425, 428, 430, 432, 436–438, 477–479, 485
resonance fluorescence 63
rotational statistical sum 200
rotational temperature 154, 169–171, 179, 184, 188–190, 200, 205, 216, 218, 230
Rydberg atom 323, 326, 329

s

Saha-Boltzmann formula 9
satellite branche 511, 512, 521, 550, 561
satellite intensity ratio 317, 319, 321
saturation power density 86, 87
scattering cross-section per unit volume 375
scattering region 378, 379, 386
scattering signal 375, 378, 388, 390
selection rule 508, 510, 512, 518, 519, 532, 535, 537, 546, 561
sensitivity 414, 461–470, 473–476, 478
series of dielectric layers 405
sharpness factor 419
shift cross section 36, 42
skin layer 399, 400
slit instrument 409, 410, 432
solar constant 30
solar photosphere 301, 303
source function 154
spectra of a discharge in an He-Ne mixture 122
spectral absorption coefficient 44, 45, 54
spectral analysis methods 235
spectral density of radiance 28
spectral intensity 12, 16
spectral line profile 31, 33, 36, 38, 42
spectral profile of the Thomson scattering 376
spectrum of fluctuations 374
spectrum inversion 211–216
spin splitting 488
spontaneous Raman scattering 130, 133, 134, 136, 140, 141
standard sources 583
Stark effect for multielectron atoms 327
Stark multiplet 312, 323, 325, 328, 335
Stark spectroscopy 307, 322, 323, 334–336, 341, 347, 348
statistical sum 7–9
statistical weight 7
statistical weight for rotational levels 491
statistical weight of rotational level of molecules 489
statistical weight of rotational levels 491
statistical weight of the levels 6

statistical weight of the vibrational level 489
statistical wing 38, 42
Stefan–Boltzmann law 11
Stern–Fulmer plots 113
stimulated Raman scattering 135–137, 140
strongly ionized plasma 2, 3
sub-Doppler Stark spectroscopy 336
surface brightness 583
Swan bands 190
symmetry number 490
symmetry operation 491

t

thermal noise 462, 465, 466
thermal photodetector 461, 462, 465, 470, 471
thermodynamic equilibrium 5, 6, 14, 15, 20, 25
thermoelement 464, 465
thermoplastic techniques 479
third-order susceptibility 137
Thomas–Reiche–Kuhn sum rule 45
Thomson and collective 377–379, 386
time coherence 92
tomographic problem 71
torsional vibrations 494
transfer of radiation 16
translational temperature 19
transparency of the optical system 412
Treanor distribution 195, 196
two isolated levels approximation 308
two- and three-quantum transition 209
two-level scheme 107, 112
two-photon absorption cross section 132, 133
two-photon absorption optogalvanic spectroscopy 125
two-photon Lamb dip optogalvanic spectroscopy 124
two-photon transition 131
two-tube method 75, 78–80
types of fluctuations 377

v

van Held ‘growth curves’ 48
velocity of the ion 165
Vibrational distributions of the CO molecules 203, 210
vibrational level 174, 191–194, 196, 199, 202, 204, 205, 207, 209, 214, 219, 224, 231, 233
vibrational temperature 191, 193, 199, 200, 202, 205, 212–214, 219, 221–223, 233
virtual state 130, 134
Voigt profile 42, 43, 48
Volterra integral equation 73
volume spectral density 12
volumetric source 584–586, 588

w

weak coupling approximation 385
weakly ionized plasma 2–4
Weisskopf radius 34, 35
White cell 95
width of the principal diffraction maximum 411
widths at half-maximum of the H_α and H_β lines 362

z

Zeeman effect 311, 343, 344